RSC Advances

PAPER

View Article Online
View Journal | View Issue

Cite this: *RSC Adv.*, 2023, **13**, 16529

Magnetocaloric effect and critical behavior of the $La_{0.75}Ca_{0.1}Na_{0.15}MnO_3$ compound

Souhir Bouzidi, *[a] Mohamed Hsini,[b] Sonia Soltani,[c] Manel Essid,[d] M. A. Albedah,[e] Hafedh Belmabrouk [e] and J. Dhahri[a]

Received 12th April 2023
Accepted 17th May 2023

DOI: 10.1039/d3ra02443a

rsc.li/rsc-advances

In this paper, we have studied the critical behavior and the magnetocaloric effect (MCE) simulation for the $La_{0.75}Ca_{0.1}Na_{0.15}MnO_3$ (LCNMO) compound at the second order ferromagnetic–paramagnetic phase transition. The optimized critical exponents, based on the Kouvel–Fisher method, were found to be: $\beta = 0.48$ and $\gamma = 1$. These obtained values supposed that the Mean Field Model (MFM) is the proper model to analyze adequately the MCE in the LCNMO sample. The isothermal magnetization $M(H, T)$ and the magnetic entropy change $-\Delta S_M(H, T)$ curves were successfully simulated using three models, namely the Arrott–Noakes equation (ANE) of state, Landau theory, and MFM. The framework of the MFM allows us to estimate magnetic entropy variation in a wide temperature range within the thermodynamics of the model and without using the usual numerical integration of Maxwell relation.

1 Introduction

The ferromagnetic (FM)–paramagnetic (PM) second-order phase transition is one of the most advanced issues in terms of functionality and fundamental physics of magnetic materials. As an advanced research interest, it is important to analyze the magnetocaloric effect when evaluating the effectiveness of magnetic refrigerators, which should be more economical and environmentally friendly.[1–3] Therefore, the second-order ferromagnetic–paramagnetic phase transition may be discussed based on the concept of critical behavior that links several thermodynamic properties of the magnetic system.

Around the FM–PM, various phase-transition measurable quantities can be determined using a series of critical exponents defining the behavior of these magnetic materials.[4–7] The design and development of magnetic refrigeration devices require a solid thermodynamic description of the magnetic system, as well as its characteristics during each phase of the refrigeration cycle. Recently the magnetic properties and the magnetocaloric effect (MCE) for $La_{0.75}Ca_{0.1}Na_{0.15}MnO_3$ (LCNMO) manganite undergoing a second order (SO) FM–PM phase transition, were reported in our previous work.[8] Near room temperature, the LCNMO sample exhibits a large magnetic entropy change with maxima of 4.83 J kg^{-1} K^{-1} and a high relative cooling power of 230 J kg^{-1} under 5 T magnetic field. These results suggest that the LCNMO sample could be promising candidates for magnetic refrigeration.

Several numerical methods[9–12] can be exploited to solve the non-algebraic equation relating the magnetization $M(H, T)$ to the applied magnetic field H and the temperature T in the ferromagnetic material. The utility of theoretically efficient methods can be exploited to simplify data analysis. However, the magnetic entropy change, $-\Delta S_M(H, T)$ is governed by H, T, the magnetic field variation (ΔH), the temperature variation (ΔT) and $M(H, T)$ data. As a result, choosing H, T, ΔH, and ΔT is important during evaluating the MCE of the magnetic material.

In this work, the critical behavior of LCNMO has been studied. Firstly, the critical exponents β and γ were calculated by an iterative method extended to the modified Arrot plot (MAP). The inverse of the magnetic susceptibility $\chi_0^{-1}(T)$ and the spontaneous magnetization $M_s(T)$ were determined. Then, isothermal $M(H, T)$ and $-\Delta S_M(T)$ curves were generated by resolving the Arrott–Noakes equation (ANE) of state. Secondly, the use of the Landau model of phase transitions[13–15] enables the simulation of $M(H, T)$ and $-\Delta S_M(T)$ curves. However, these two approaches (ANE and Landau theory) are valid only in a very narrow temperature region near the Curie temperature, T_C. Thirdly, by analyzing the mean field equation, the $M(H, T)$ and $-\Delta S_M(T)$ plots of our studied LCNMO magnetic system are generated. Contrarily to what has been mentioned about the ANE and the Landau model, the dependence of M and $-\Delta S_M$ on T, H can be described by using the Mean Field Model (MFM) in a large temperature region.

[a]*Laboratoire de La Matière Condensée et des Nanosciences, Département de Physique, Faculté des Sciences de Monastir, Avenue de L'Environnement Monastir, 5019 Monastir, Tunisia. E-mail: Souhirbouzidi@outlook.com*

[b]*Laboratory of Physical Chemistry of Materials, Faculty of Science of Monastir, Department of Physics, University of Monastir, 5019 Monastir, Tunisia*

[c]*Department of Physics, College of Science and Arts, Qassim University, Dariyah 58251, Saudi Arabia*

[d]*Chemistry Department, College of Science, King Khalid University (KKU), P.O. Box 9004, Abha, Saudi Arabia*

[e]*Department of Physics, College of Science, Majmaah University, Al Majma'ah, 11952, Saudi Arabia*

2 Results and discussions

The LCNMO manganite[8] was prepared by the flux method. The crystallographic study revealed that the LCNMO compound is characterized by the coexistence of a mixture of orthorhombic and rhombohedral structures with *Pbnm* and $R\bar{3}c$ space groups, respectively. The magnetization data, under 0.05 T magnetic field proved that LCNMO exhibited a SO FM–PM near the room temperature ($T_C = 301.5$ K).

2.1 Arrott–Noakes equation (ANE)

Overall, the ANE near the second-order ferromagnetic–paramagnetic transition is expressed as:[16]

$$\left(\frac{H}{M}\right)^{\frac{1}{\gamma}} = a(T - T_C) + bM^{\frac{1}{\beta}} \quad (1)$$

It involves two constants, namely a and b and two critical coefficients, namely γ and β.

Using the thermodynamic relation $\left.\frac{\partial S}{\partial M}\right|_T = \left.\frac{\partial H}{\partial T}\right|_M$, the expression of $-\Delta S_M(M)$ is given through eqn (1) by:[17]

$$-\Delta S_M(M) = \int_{M_s}^{M} a\gamma M \left(bM^{\frac{1}{\beta}} + a(T - T_C)\right)^{\gamma-1} \mathrm{d}M \quad (2)$$

Basing on eqn (1), the initial magnetic susceptibility χ_0 for $T > T_C$ and the spontaneous magnetization M_S for $T < T_C$ are as follows:[18]

$$M_S = M_0(-\varepsilon)^{\beta};\ T < T_C, \quad (3)$$

$$\chi_0^{-1} = h_0\varepsilon^{\gamma};\ T > T_C, \quad (4)$$

$$M = R_0 H^{\left(\frac{1}{\delta}\right)};\ \ T = T_C, \quad (5)$$

where $\delta = 1 + \frac{\gamma}{\beta}$, $\varepsilon = \frac{T - T_C}{T}$ is the reduced temperature, M_0, h_0 and R_0 present critical amplitudes. The choice of β and γ values is adequate if it results in a parallel set of linear lines for the plot $M^{\frac{1}{\beta}}$ *vs.* $\left(\frac{H}{M}\right)^{\frac{1}{\gamma}}$ with the passing of the critical isotherm (at $T = T_C$) from the origin. For $T < T_C$, the abscissa intercepts correspond to $M_S^{1/\beta}$ however for $T > T_C$, the ordinate intercepts refer to $(\chi_0^{-1})^{1/\gamma}$. The involvement of arbitrary critical exponents in eqn (1) may conduct to unacceptable fits and erroneous values of the exponents. For this reason, an implemented program based on a rigorous iterative method[19] is often used to determine the values of the couple (β, γ) after starting with the initial MFM critical values ($\beta = 0.5$, $\gamma = 1$). After multiple iterations, a set of nearly parallel straight lines $M^{\frac{1}{\beta}}$ *vs.* $\left(\frac{H}{M}\right)^{\frac{1}{\gamma}}$ have been generated. In Fig. 1, we report the curves using the values: $\beta = 0.48$ and $\gamma = 1$.

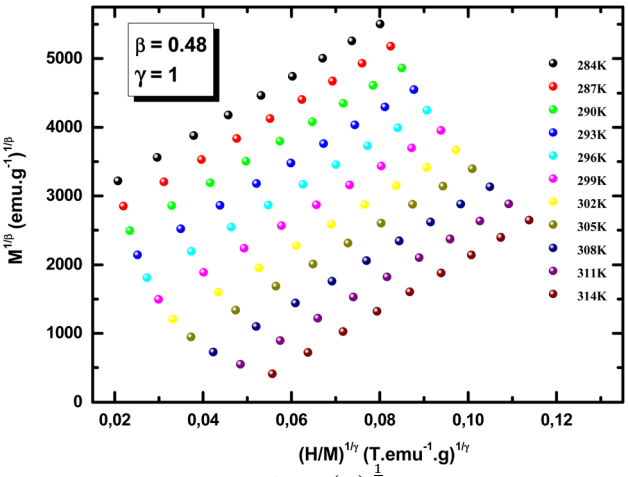

Fig. 1 Modified Arrot plot, $M^{\frac{1}{\beta}}$ *vs.* $\left(\frac{H}{M}\right)^{\frac{1}{\gamma}}$, for $La_{0.75}Ca_{0.1}Na_{0.15}MnO_3$ (LCMNO) compound.

It is evident in Fig. 1 that isothermal lines $M^{\frac{1}{\beta}}$ *vs.* $\left(\frac{H}{M}\right)^{\frac{1}{\gamma}}$ were set under high magnetic fields (greater than $H = 1$ T). This is because isotherms are averaged and magnetized in different directions at lower magnetic fields.[20] But, under high magnetic fields, all isotherms undergo parallel straight lines. The values of the critical exponent of LCMNO are close to those predicted by the MFM ($\beta = 0.5$, $\gamma = 1$). Linear fits of the MAP yield the M_S1/β and $(\chi_0^{-1})^{1/\gamma}$ described above. The estimated data of $M_S(T)$ and $\chi_0^{-1}(T)$ are plotted in Fig. 2(a). Fitting $M_S(T)$ using eqn (3) gives the values of: $\beta = 0.48$ and $T_C = 301.49$ K. Similarly, fitting $\chi_0^{-1}(T)$ using eqn (4) gives: $\gamma = 1$ and $T_C = 301.5$ K. Since the experimental data of the critical isotherm $M(H)$ at $T_C = 301.5$ K is not available, the critical exponent δ is supposed to be restricted between $M(H)$ at 299 and 302 K. temperature. The fit of the isotherms $M(H, T = 299\ \mathrm{K})$ and $M(H, T = 302\ \mathrm{K})$ with eqn (5) gives the respective values of δ as 3.46 and 2.86. Furthermore, this δ exponent may be also calculated from Widom scaling relation:[21] $\delta = 1 + \frac{\gamma}{\beta}$. With the optimized values, $\beta = 0.48$ and $\gamma = 1$, $\delta = 3.08$. It is obvious that the δ value is restricted between the ones calculated from the fit of isotherms $M(H, T = 299\ \mathrm{K})$ and $M(H, T = 302\ \mathrm{K})$ with eqn (5). As a result, the reliability of the estimated critical exponents was confirmed.

For the LCMNO compound, the γ value matches the MFM suggesting that the FM–PM phase transition would belong to the MFM. Thus, the origin of this transition is explained by the long-range physical interaction. Moreover, for a system of dimension d and spin n, γ varies with extension of the interaction σ as:[22] $\gamma = 1 + \frac{4}{d}\left(\frac{n+2}{n+8}\right)\Delta\sigma + \frac{4(8n-4)(n+2)}{d^2(n+8)^2}\left[1 + \frac{2G\left(\frac{1}{2}d\right)(7n+20)}{(n-4)(n+8)}\right]\Delta\sigma^2$ with $\Delta\sigma = \sigma - \frac{d}{2}$; $G\left(\frac{1}{2}d\right) = 3 - \frac{1}{4}\left(\frac{1}{2}d\right)^2$. The renormalization group study

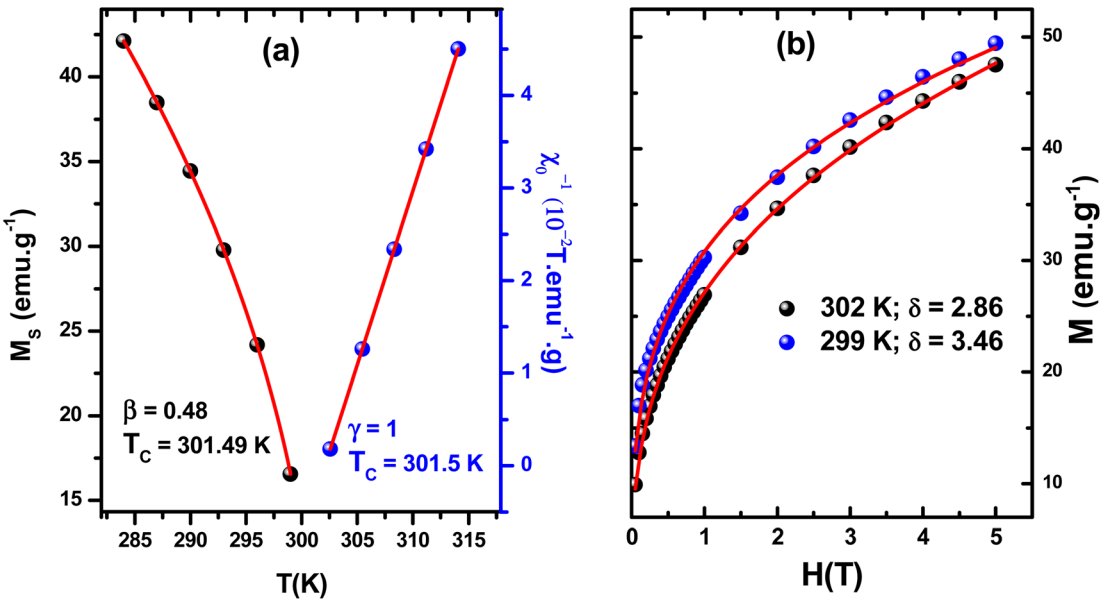

Fig. 2 (a) Fitting of $M_S(T)$ and $\chi_0^{-1}(T)$, with eqn (3) and (4), respectively. (b) Fitting of $M(H)$ at 299 and 302 K temperature with eqn (5), for LCMNO sample.

suggests that σ (or γ) indicates the exchange integral $J(r)$ over a distance r as follows:[23] $J(r) \sim r^{-(d+\sigma)}$. For $\sigma > 2$ or $\sigma < 2$, we observe a 3D system of isotropic long- or short-range spins, respectively. The 3D Heisenberg model is correct if $\sigma > 2$, with $J(r)$ decreasing at short distances faster than r^{-5}. In our case (with $\gamma = 1$), $\sigma \approx 1.5$; then $J(r)$ decreases as $r^{-4.5}$. Therefore, $J(r)$ decreases more slowly than r^{-5} for LCMNO manganite as a function of long-range distance.

To simulate $M(H, T)$ and $-\Delta S_M(T, H)$ curves, around T_C, we have first determined the constants a and b given in eqn (1) were firstly determined. The linear fits of $\left(\frac{H}{M}\right)^{\frac{1}{\gamma}}$ *vs.* $M^{\frac{1}{\beta}}$ yield $a(T - T_C)$ at the interceptions of the axis $\left(\frac{H}{M}\right)^{\frac{1}{\gamma}}$. The quantity b represents the slope of $\left(\frac{H}{M}\right)^{\frac{1}{\gamma}}$ *vs.* $M^{\frac{1}{\beta}}$ at T_C. Both constants are calculated as: $a = 0.0036$ and $b = 2.6\ 10^{-5}$ with units of M in emu g^{-1} and H in tesla.

Then the numerical resolution of eqn (1) generates $M(H, T)$ plots (solid lines). A good agreement is observed with the experimental data mainly when H is greater than 1 T as presented in Fig. 3(a).

Using $M_S(T)$ and the generated values of $M(H, T)$, a theoretical estimation of $-\Delta S_M(T, H)$ can be obtained. These simulated $-\Delta S_M$ curves (solid lines) correlated adequately with experimental $-\Delta S_M$ curves which were evaluated using the well-known Maxwell relation $-\Delta S_M(T, H) = -\int_{H_1}^{H_2} \left(\frac{\partial M}{\partial T}\right)_H dH$, as shown in Fig. 3(b). Although a reasonable correlation was obtained in the whole temperature, the simulated curves of $-\Delta S_M(T)$ depart slightly from the experimental ones near T_C. This shift is consistent with saturation effects not contemplated in the ANE.[24]

2.2 Landau theory

According to the Landau model, the Gibbs free energy can be written as follows:[25]

$$G(T, M) = G_0 + \frac{1}{2}A(T)M^2 + \frac{1}{4}B(T)M^4 + \frac{1}{6}C(T)M^6 - MH \quad (6)$$

where $A(T)$, $B(T)$ and $C(T)$ are Landau parameters depending on temperature. In the equilibrium condition, $\partial G/\partial M = 0$, the magnetic equation is derived as:

$$\frac{H}{M} = A(T) + B(T)M^2 + C(T)M^4 \quad (7)$$

The variables $A(T)$, $B(T)$ and $C(T)$ can be calculated from the quadratic fit of *vs.* M^2.

The magnetic entropy is given as follows:

$$-\Delta S_M(T, M) = \left(\frac{\partial G(H, T)}{\partial T}\right)_H = -\frac{1}{2}A'M^2 - \frac{1}{4}B'M^4 - \frac{1}{6}C'M^6 \quad (8)$$

where $A' = \frac{\partial A}{\partial T}$, $B' = \frac{\partial B}{\partial T}$ and $C' = \frac{\partial C}{\partial T}$.

Using the renormalization group, Dong *et al.*[26] pointed out that in the absence of the external magnetic field, $-\Delta S_M(H = 0$ T) should differ from zero since it is impacted by spontaneous magnetization. Therefore, eqn (8) should be adjusted as follows:

$$-\Delta S_M(T, M) = -\frac{1}{2}A'(M - M_S)^2 - \frac{1}{4}B'(M - M_S)^4 - \frac{1}{6}C'(M - M_S)^6 \quad (9)$$

The treatment of eqn (6) leads to the generation of $M(H, T)$ plots which are represented by red lines and corroborate the

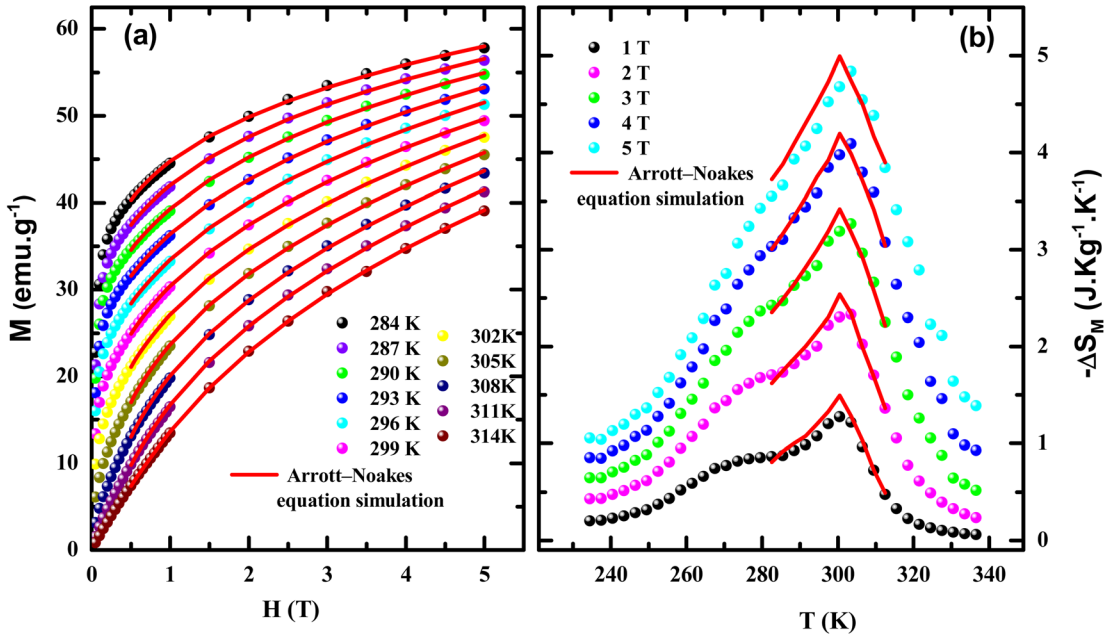

Fig. 3 The experimental (red lines) and the simulated (symbols) curves of (a) M *vs.* H and (b) $-\Delta S_M$ *vs.* T using the ANE.

experimental data when H is larger than 0.5 T as indicated in Fig. 4(a). Then, using generated $M(H, T)$, obtained from eqn (6), and $M_S(T)$ in eqn (8), simulated $-\Delta S_M$ curves can be determined. An acceptable concordance is achieved between the simulated $-\Delta S_M$ curves (red lines) and the experimental $-\Delta S_M$ curves (symbols) estimated by Maxwell's relations as given in Fig. 4(b).

Some points can be discussed when comparing the ANE with its derivatives from one side and the Landau theory from the other side. These two approaches are valid only in a very narrow region: $|\varepsilon| < 0.1$.[27] Since the critical behavior at the second FM–PM phase transition is studied at high magnetic field, under weak magnetic fields, the ANE has a limited ability to simulate the curves of magnetic compounds (in this study), we take the analysis starting from 1 T because of the inability to obtain parallel straight lines $M^{\frac{1}{\beta}}$ *vs.* $\left(\frac{H}{M}\right)^{\frac{1}{\gamma}}$ for the total applied magnetic field. Landau theory (which starts at 0.5 T) decreases

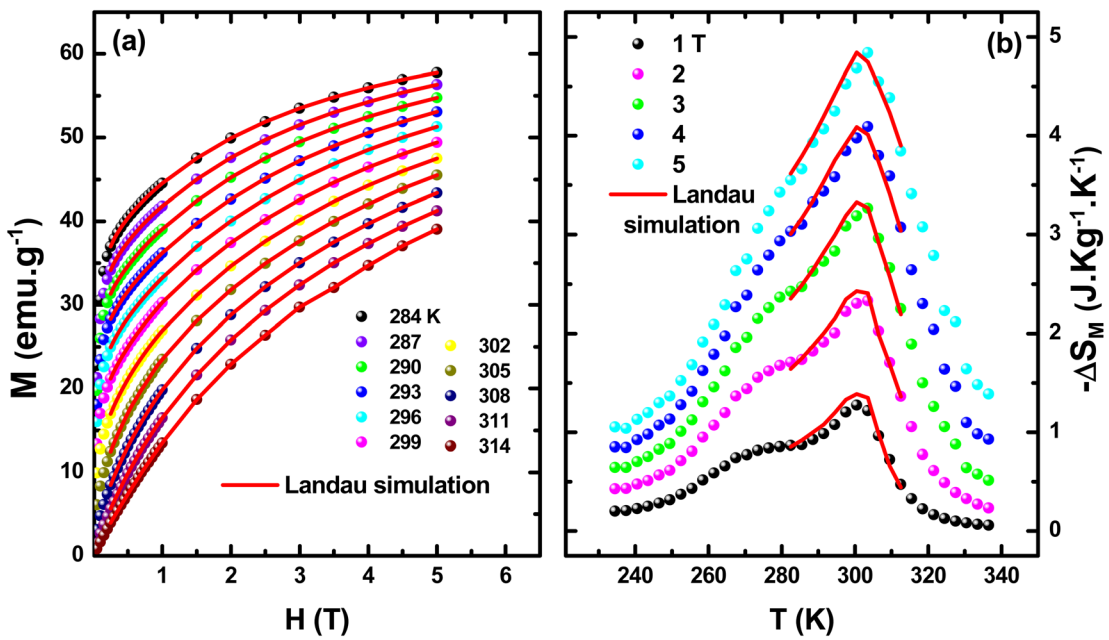

Fig. 4 The experimental (symbols) and the simulated (red lines) curves of (a) M *vs.* H and (b) $-\Delta S_M$ *vs.* T using the Landau theory.

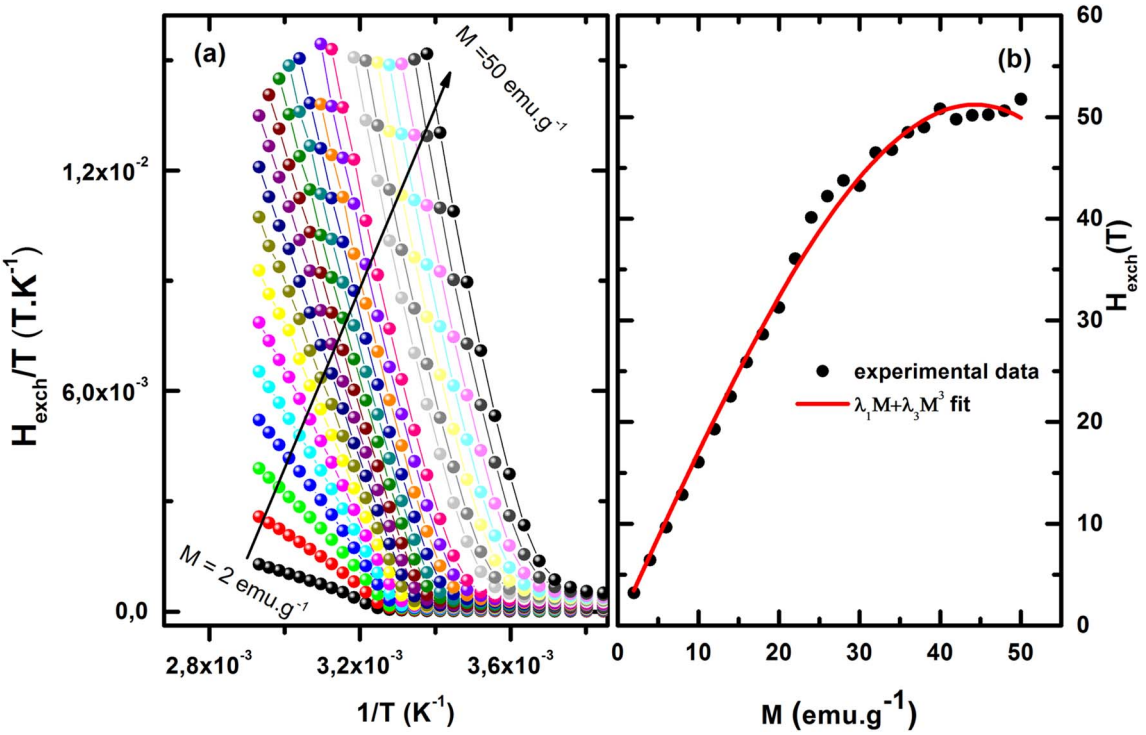

Fig. 5 (a) Evolution of $\frac{H}{T}$ *vs.* $\frac{1}{T}$ with 2 emu g^{-1} step plot (b) fitting H_{exch} *vs.* M.

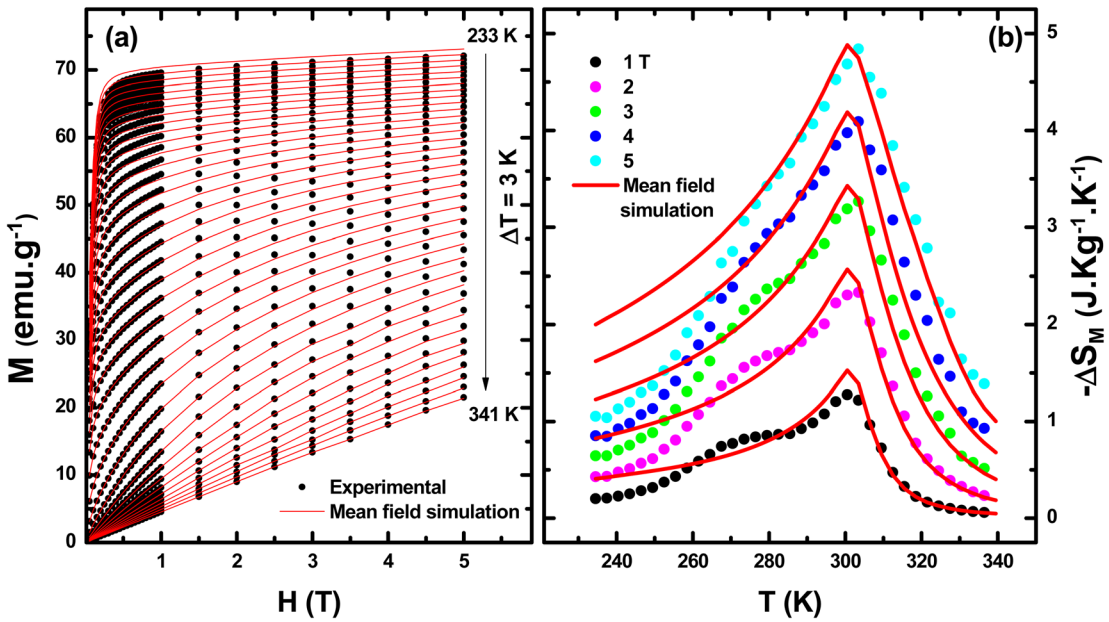

Fig. 6 The experimental (symbols) and the simulated (red lines) curves of (a) M *vs.* H and (b) $-\Delta S_M$ *vs.* T using the MFM.

this disability but is still unable to simulate $M(H, T)$ curves under low magnetic fields.

$$M(H,T) = M_0\left[\frac{2J+1}{2J}\coth\left(\frac{2J+1}{2J}\frac{Jg\mu_B}{k_B}\left(\frac{H+H_{exch}}{T}\right)\right) - \frac{1}{2J}\coth\left(\frac{1}{2J}\frac{Jg\mu_B}{k_B}\left(\frac{H+H_{exch}}{T}\right)\right)\right] \quad (10)$$

2.3 Mean field model

The magnetization values can be expressed according to the MFM with respect to the saturation magnetization (M_0) as[28,29] where μ_B is the Bohr magnetron, g is the gyromagnetic factor, k_B is the Boltzmann constant, J is the total angular momentum, and H_{exch} is the exchange magnetic field which is given

according to Weiss[30] as $\vec{H}_{exch} = \lambda\vec{M}$, λ is the exchange parameter.

Knowing that M is a function of $\frac{H + H_{exch}}{T}$; in other words, $M(T,H) = f\left(\frac{H + H_{exch}}{T}\right)$, we may obtain the relation:

$$\frac{H}{T} = f^{-1}(M) - \frac{H_{exch}}{T} \quad (11)$$

Then, ΔS_M between two magnetic fields $H_1 \rightarrow H_2$ can be estimated theoretically as follows:[31]

$$\Delta S_M(T)_{H_1 \rightarrow H_2} = -\int_{M|_{H_1}}^{M|_{H_2}} \left(f^{-1}(M) - \left(\frac{\partial\lambda(T)}{\partial T}\right)_M M\right) dM \quad (12)$$

From the $M(H, T)$ curves evaluated at constant values of magnetization M with a step of 2 emu g^{-1}, the evolution of $\frac{H}{T}$ as a function of $\frac{1}{T}$ was plotted in Fig. 5(a). A linear behavior of the isomagnetic curves of $\frac{H}{T}$ *versus* $\frac{1}{T}$ is observed. The lines gradually shift to larger values of the temperature. It is worth studying the H_{exch} to sort out the value of the mean-field exchange parameter λ. From eqn (11), the slopes of $\frac{H}{T}$ *vs.* $\frac{1}{T}$ give the H_{exch}. Then, H_{exch} *versus* M was plotted in Fig. 5(b). Knowing that magnetization is an odd function of the exchange magnetic field:[32]

$$H_{exch} = \lambda_1 M + \lambda_3 M^3 \quad (13)$$

Then, H_{exch} as a function of M in Fig. 5(b) was fitted by eqn (13). A very low dependence on M^3 was noted ($\lambda_3 = -0.0003$ (T emu^{-1} g)^3). One can consider $H_{exch} = \lambda_1 M \approx \lambda M$, with $\lambda_1 = 1.73$ T emu^{-1} g.

For $La_{0.75}Ca_{0.1}Na_{0.15}MnO_3$ manganite, using the Hund rules in ref. **30**, $J = g = 2$. The saturation magnetization is given by fitting $M(H, T)$ *vs.* $\frac{H + H_{exch}}{T}$ with eqn (10) (not shown here) and its value is found to be $M_0 = 103.9$ emu g^{-1}.

Adding parameters λ, J, g and M_0 to eqn (10) enables the generation of $M(H, T)$ curves (red lines) which are plotted in in Fig. 6(a) with experimental $M(H, T)$ data (black symbols). A good agreement between the calculated and the experimental plots of $M(H, T)$ was found.

Fig. 6(b) shows the comparison between the $-\Delta S_M$ curves using the MFM (red lines) from exploiting eqn (12) and the related experimental data (solid symbols) by using Maxwell's relation. The entropy results show a good agreement between simulated and experimental $-\Delta S_M$ curves in the PM region but some notable discrepancies, especially in the FM range. These discrepancies may be associated with the high spontaneous magnetization in the FM area; the phase transition is far from the area of interest. In fact, this $M_S(T)$ obeys eqn (3) for a temperature range far from the transition where the ANE is not valid. When integrating eqn (2), $M_S(T)$ has been eliminated. But eqn (12) does not mention $M_S(T)$. This could be explained by the fact that the MFM is not able to accurately describe the magnetization and magnetic entropy in these temperature ranges (far from T_C).[33] In addition, some deviations of the simulated entropy results near T_C may be associated to the fact that the MFM does not consider fluctuations and disorder effects (chemical and structural inhomogeneity) near T_C.[34]

3 Conclusion

In conclusion, three models were exploited to investigate the MCE of $La_{0.75}Ca_{0.1}Na_{0.15}MnO_3$ (LCNMO) manganite. The ANE was analyzed to determine the critical exponents of the LCNMO magnetic system. The deduced critical exponents are found to be as: $\beta = 0.48$ and $\gamma = 1$. A close relationship between these estimated critical exponents and those identified by the Mean Field Model (MFM) with $\beta = 0.5$ and $\gamma = 1$. An excellent agreement exists between the simulated and the experimental curves of the isothermal magnetization $M(H, T)$ and the magnetic entropy change $-\Delta S_M(T)$ curves using the ANE and the Landau model near the FM–PM transition but in a short temperature range. Considering that the MFM may be adequate to analyze the MCE in LCNMO magnetic system, a good correlation was found between the $M(H, T)$ and $-\Delta S_M(T)$ curves generated by the MFM and the corresponding experimental data. The results of this MFM scaling method are very promising for a SO magnetic system. Moreover, it is interesting to emphasize that this analysis is global, in the sense that it encompasses the consistency of the whole range magnetization data.

Data availability

The datasets generated or analysed during the current study are available from the corresponding author on reasonable request.

Author contributions

The manuscript was written with the contributions of all authors. SB contributed to preparing experimental data. MH contributed to calculations. SS and ME contributed to editing of the manuscript. MAA and HB contributed to reviewing and editing of the manuscript. JD contributed to review of the manuscript and supervising.

Conflicts of interest

There are no conflicts to declare.

Acknowledgements

The authors extend their appreciation to the Deanship of Scientific Research at King Khalid University for funding this work through large group Research Project under grant number RGP2/110/44.

References

1 Z. Ma, P. Xu, J. Ying, Y. Zhang and L. Li, *Acta Mater.*, 2023, **247**, 11875.
2 Y. Zhang, J. Zhu, S. Li, Z. Zhang, J. Wang and Z. Ren, *Sci. China Mater.*, 2022, **65**, 1345–1352.
3 Y. Zhang, Y. Tian, Z. Zhang, Y. Jia, B. Zhang, M. Jiang, J. Wang and Z. Ren, *Acta Mater.*, 2022, **226**, 117669.
4 D. Guo, L. M. Moreno-Ramírez, J. Law, Y. Zhang and V. Franco, *Sci. China Mater.*, 2023, **66**, 249–256.
5 P. Xu, L. Hu, Z. Zhang, H. Wang and L. Li, *Acta Mater.*, 2022, **236**, 118114.
6 Y. Zhang, P. Xu, J. Zhu, S. Yan, J. Zhang and L. Li, *Mater. Today Phys.*, 2023, **32**, 101031.
7 L. Li and M. Yan, *J. Mater. Sci. Technol.*, 2023, **136**, 1–12.
8 S. Bouzidi, M. A. Gdaiem, J. Dhahri and E. K. Hlil, *RSC Adv.*, 2019, **9**, 65–76.
9 A. S. Erchidi Elyacoubi, R. Masrour and A. Jabar, *Solid State Commun.*, 2018, **271**, 39–43.
10 N. H. van Dijk, *J. Magn. Magn. Mater.*, 2021, **529**, 167871.
11 M. Hsini, S. Hcini and S. Zemni, *J. Magn. Magn. Mater.*, 2018, **466**, 368–375.
12 M. Hsini, S. Hcini and S. Zemni, *Eur. Phys. J. Plus*, 2019, **134**, 588.
13 A. Fujita and K. Fukamichi, *IEEE Trans. Magn.*, 2005, **41**, 3490–3492.
14 V. S. Amaral, J. P. Araújo, Yu. G. Pogorelov, P. B. Tavares, J. B. Sousa and J. M. Vieira, *J. Magn. Magn. Mater.*, 2002, **242–245**, 655–658.
15 V. S. Amaral, *et al.*, *J. Appl. Phys.*, 2003, **93**, 7646.
16 A. Arrott and J. E. Noakes, *Phys. Rev. Lett.*, 1967, **19**, 786.
17 V. Franco and A. Conde, *Int. J. Refrig.*, 2010, **33**, 465.
18 M. E. Fisher, *Rep. Prog. Phys.*, 1967, **30**, 615.
19 V. Franco, J. S. Blazquez and A. Conde, *Appl. Phys. Lett.*, 2006, **89**, 222512.
20 V. Franco, A. Conde, J. M. Romero-Enrique and J. S. Blazquez, *J. Phys.: Condens. Matter*, 2008, **20**, 285207.
21 B. Widom, *J. Chem. Phys.*, 1965, **43**, 3898.
22 A. Aharoni, *Introduction to the Theory of Ferromagnetism*, Clarendon Press, Oxford, 1996, ch. 4.
23 A. K. Pramanik and A. Banerjee, *Phys. Rev. B: Condens. Matter Mater. Phys.*, 2009, **79**, 214426.
24 C. Romero-Muniz, J. J. Ipus, J. S. Blazquez, V. Franco and A. Conde, *Appl. Phys. Lett.*, 2014, **104**, 252405.
25 V. S. Amaral and J. S. Amaral, *J. Magn. Magn. Mater.*, 2004, **272–276**, 2104–2105.
26 Q. Y. Dong, H. W. Zhang, J. L. Shen, J. R. Sun and B. G. Shen, *J. Magn. Magn. Mater.*, 2007, **319**, 56.
27 L. Zhang, J. Fan and Y. Zhang, *Mod. Phys. Lett. B*, 2014, **28**, 1450059.
28 J. Coey, *Magnetism and Magnetic Materials*, Cambridge University Press, Cambridge, 2009.
29 J. A. Gonzalo, *Effective Field Approach to Phase Transitions and Some Applications to Ferroelectrics*, World Scientific, Singapore, 2006.
30 C. Kittel, *Introduction to Solid State Physics*, John Wiley and Sons, New York, 7th edn, 1996.
31 J. S. Amaral, N. J. O. Silva and V. S. Amaral, *Appl. Phys. Lett.*, 2007, **91**, 172503.
32 S. B. Ogale, R. Shreekala, R. Bathe, S. K. Date, S. I. Patil, B. Hannoyer, F. Petit and G. Marest, *Phys. Rev. B: Condens. Matter Mater. Phys.*, 1998, **57**, 7841.
33 B. Mohamed, F. Allab, C. Dupuis, D. Fruchart, D. Gignoux, *et al.*, Analysis and modeling of magnetocaloric effect near magnetic phase transition temperature, in *Second IIF-IIR International Conference on Magnetic Refrigeration at Room Temperature*, Portoroz, Slovenia, 2007.
34 J. S. Amaral, P. B. Tavares, M. S. Reis, J. P. Araújo, T. M. Mendonça, V. S. Amaral and J. M. Vieira, *J. Non-Cryst. Solids*, 2008, **354**, 5301–5303.